AMERICAN ACADEMY OF OPHTHALMOLOGY®

Relationship between Three-Dimensional Magnetic Resonance Imaging Eyeball Shape and Optic Nerve Head Morphology

Kyoung Min Lee, MD,[1,2,*] *Sun-Won Park, MD,*[3,4,*] *Martha Kim, MD,*[5] *Sohee Oh, PhD,*[6] *Seok Hwan Kim, MD*[1,2]

Purpose: To determine if the 3-dimensional (3D) eyeball shape is associated with the positions of the central retinal vascular trunk (CRVT) and the externally oblique border (EOB) in the optic nerve head (ONH).

Design: Prospective, cross-sectional study.

Participants: Fifty-six subjects (112 eyes) with a diagnosis of glaucoma or glaucoma suspect.

Methods: The eyeball shape on 3D magnetic resonance imaging (MRI) scans was classified according to the dimension of the longest diameter: axial dimension (prolate sphere), group 1; horizontal dimension (horizontally oblate sphere), group 2; and vertical dimension (vertically oblate sphere), group 3. The deviation of the CRVT, as a surrogate of lamina cribrosa (LC) shift, was measured from the center of the Bruch's membrane opening (BMO) demarcated by OCT imaging, with the horizontal midline as 0° and the superior location as a positive value. The angular location of the longest EOB was also measured.

Main Outcome Measure: Positions of CRVT and EOB according to the 3D eyeball shape.

Results: Among 112 eyes, 54 (48%) had a prolate shape (group 1), 23 (21%) had a horizontally oblate shape (group 2), and 35 (31%) had a vertically oblate shape (group 3). The angular deviation of the CRVT differed among the groups: to the nasal side in group 1, to the temporal side in group 2, and along the vertical meridian in group 3. In cases of asymmetric eyeball shape, the CRVT was deviated toward the undergrown side from the overgrown side, regardless of grouping. The angular location of the longest EOB was in the direction opposite to the CRVT position ($P < 0.001$). A generalized estimating equation analysis revealed that the temporal location of the CRVT was associated with older age ($P = 0.001$), nasal location of the longest EOB ($P < 0.001$), and oblate shape of the eyeball ($P < 0.001$, group 2; $P = 0.007$, group 3).

Conclusions: The position of the CRVT and EOB were associated with the 3D eyeball shape. Considering that infant ONH morphology is highly uniform, various modes of eyeball expansion during growth can result in diverse directionalities of offset between the LC and the BMO in adults. *Ophthalmology 2021;128:532-544* © *2020 by the American Academy of Ophthalmology*

Supplemental material available at www.aaojournal.org.

Retinal ganglion cells (RGCs) convey visual signals from photoreceptors to the lateral geniculate nucleus of the brain. For this purpose, the axons of RGCs escape from the closed wall of the eyeball through the exit: the optic nerve head (ONH). Notably, the funduscopic appearance of each ONH is highly variable.[1] Moreover, ONH morphology has clinical significance due to its close association with glaucomatous optic neuropathy.[2-4] Specifically, the morphology of the ONH (ovality or torsion),[5-7] locations of the central retinal vascular trunk (CRVT), and β-zone parapapillary atrophy (PPA)[3,4] have been reported to be associated with such susceptibility. Considering that the ONH morphology of newborns is highly uniform,[8] individual ONH morphology might change during eyeball growth after birth.

The Boramae Myopia Cohort Study found that the inner retinal structure of the posterior polar area, including the diameter and position of the Bruch's membrane opening (BMO), was relatively preserved during axial elongation,[9] and the outer load-bearing structure expanded.[10,11] This expansion of the sclera and the consequent shift of the lamina cribrosa (LC) from the preserved BMO resulted in the change in ONH structure that is observed in myopia: a border-tissue rotation from the internally oblique to the externally oblique direction,[9] expansion of the externally oblique border (EOB),[11] and shift of the CRVT position to the nasal side.[10] Therefore, myopic axial elongation is related to the development of the characteristic disc shape in myopia: an oval or torsional optic disc appearance with PPA and the nasal position of the CRVT.[9-11] Because the CRVT is embedded in the dense connective tissue of the LC[12] and, in most newborns, located in the central area of the ONH,[8] its deviation from the BMO center can be used for an approximate estimation of the direction and extent of LC shift.[13]

https://doi.org/10.1016/j.ophtha.2020.08.034
ISSN 0161-6420/20

The directionalities of the CRVT and EOB, however, are diverse when measured from the BMO center. The CRVT is located mostly on the nasal side of the ONH, whereas in some hyperopic eyes, it is located on the temporal side. Some eyes have an extremely vertical CRVT position. Likewise, an EOB is occasionally observed on the temporal and inferior sides,[14] and sometimes on the nasal side in nonmyopic eyes.[15] Because the CRVT is located mostly in the central area in newborns,[8] and the border between the BMO and the anterior scleral opening has mostly internal obliquity,[14] their deviations might be an acquired change during growth, as is observed in myopic eyes.[10] This supposition is supported by the following: The average axial length of newborns is approximately 17 mm,[16] which means that every eyeball longer than that must have undergone expansion during growth. Even so, according to our review of the literature, there have been no studies on the effect of eyeball growth on ONH morphology, especially in the aspect of the positions of the CRVT and EOB. The purpose of this study, correspondingly, was to determine the association between the 3-dimensional (3D) shape of the eyeball and the directionalities of the CRVT and EOB from the BMO center, which represent an offset between the LC and BMO at the ONH.

Methods

Study Participants

This investigation was based on subjects who had been enrolled in the Boramae Glaucoma Imaging Study, an ongoing prospective study at Seoul National University Boramae Medical Center (Seoul, Korea). This study registered the anatomic features of the ONH in subjects who had visited our institution with a diagnosis or suspicion of glaucoma. Between June 2019 and February 2020, volunteers who had expressed a desire for 3D magnetic resonance imaging (MRI) scans were recruited. Written informed consent to participate was obtained from all the subjects. The study protocol was approved by the Seoul National University Boramae Medical Center Institutional Review Board and conformed to the tenets of the Declaration of Helsinki.

All of the participants underwent a full ophthalmologic examination that included best-corrected visual acuity (BCVA) assessment, refraction, slit-lamp biomicroscopy, Goldmann applanation tonometry, gonioscopy, dilated funduscopic examination, keratometry (RKT-7700; Nidek, Hiroshi, Japan), axial length measurement (IOLMaster version 5; Carl Zeiss Meditec, Dublin, CA), disc photography along with red-free fundus photography (TRC-NW8; Topcon, Tokyo, Japan), and spectral-domain (SD) OCT (Spectralis OCT, Heidelberg Engineering, Heidelberg, Germany). During the acquisition of the SD-OCT images, the subjects were asked to fixate on a target, and images were acquired with the forehead and chin stabilized by the headrest. Extra care was taken during each examination to confirm that the forehead and chin were correctly positioned and did not move. Glaucomatous optic nerve damage was defined by rim thinning, notching, and the presence of retinal nerve fiber layer defects and evaluated by a glaucoma specialist (S.H.K.). Glaucomatous visual field defect was defined as (1) outside normal limits on the glaucoma hemifield test; (2) 3 abnormal points with a P value with less than a 5% probability of being normal, and 1 with a P value less than 1% by pattern deviation; or (3) a pattern standard deviation less than 5%, as confirmed on 2 consecutive reliable tests (fixation loss rate of $\leq$20%, and false-positive and false-negative error rates of $\leq$25%). Glaucoma was defined as glaucomatous optic nerve damage and associated visual field defects and classified as open-angle glaucoma and angle-closure glaucoma, depending on the irido-corneal angle status as assessed by gonioscopy.

The inclusion criterion was the willingness of subjects to undergo 3D-MRI scans for the delineation of eyeball shape. The exclusion criteria were a BCVA of <20/40, a poor-quality image (i.e., quality score <15) of any section on enhanced depth imaging (EDI) SD-OCT radial scans, a CRVT position located within the BMO but impossible to determine clearly because of vessel bifurcation, and any MRI contraindication (e.g., MRI unacceptable aneurysm clip, pacemaker, any metallic foreign body). Both eyes were used for the analysis.

Three-Dimensional Magnetic Resonance Imaging of an Eyeball

The 3D shape of the eyeball was measured as an area of high signal index on the T2-weighted 3D-MRI upon receipt of the participant's informed consent. The MRI examinations were performed at 3.0 T by using a Philips Achieva (Philips Healthcare, Best, The Netherlands). The participants were instructed to keep both eyes closed with minimal movement during the scanning. Scanning sequences (repetition time = 2500 ms; echo time = 248 ms; flip angle = 90°; field of view = 256 × 256 × 188 mm) were performed with maximum water-fat shift.[17] The image resolution was 1 × 1 × 1 mm, which was used in the classification of the eyeball shapes of high myopia.[17] Volume rendering of the images was performed by using commercially available software (OsiriX MD; Food and Drug Administration cleared, Pixmeo, Geneva, Switzerland).

Classification of the Three-Dimensional Shape of an Eyeball

The eyeball's 3D shape was determined by (1) the horizontal width along the x-axis; (2) the vertical height along the y-axis; and (3) the axial length along the z-axis (Fig 1A). Based on the deviations from the spherical shape, the classification of eyeballs was divided into 3 types: group 1, if the longest dimension was the axial length ($z \geq x$ and y; Fig 1C$_1$); group 2, if the horizontal width was ($x \geq z$ and y; Fig 1C$_2$); and group 3, if the vertical height was ($y \geq x$ and z; Fig 1C$_3$). The groups represented a prolate sphere, horizontally oblate sphere, and vertically oblate sphere, respectively.

To compare the lengths of the eyeball along the x-, y-, and z-axes, we used the 3D multiplanar reconstruction (MPR) volume-rendering tool of OsiriX (Fig 1B). In the 3D MPR mode, altering the orientation on any of the 3 planes affects the other 2 corresponding planes. Thus, rotation in MPR allows for direct measurement of the lengths across any point of an eyeball in any desired direction on the 3D reconstructed image. To define the x-, y-, and z-axes, we used a stepwise approach: (1) a presumptive center of an eyeball was pointed out on the coronal plane; (2) after centering the eyeball on the coronal plane, the key images were selected on the sagittal and transverse planes when the eyeball was visualized mostly on each plane, respectively; and (3) the measuring axes were adjusted to be perpendicular to the lens (Fig 1B). We determined which dimension had the longest length along the x-, y-, and z-axes, and accordingly, the eyeball was classified as group 1 if the longest axis was z (including x=y=z), group 2 if x (including x=y>z), and group 3 if y.

The measurements were performed with the built-in caliper of OsiriX. Two independent observers (K.M.L. and S.W.P.)

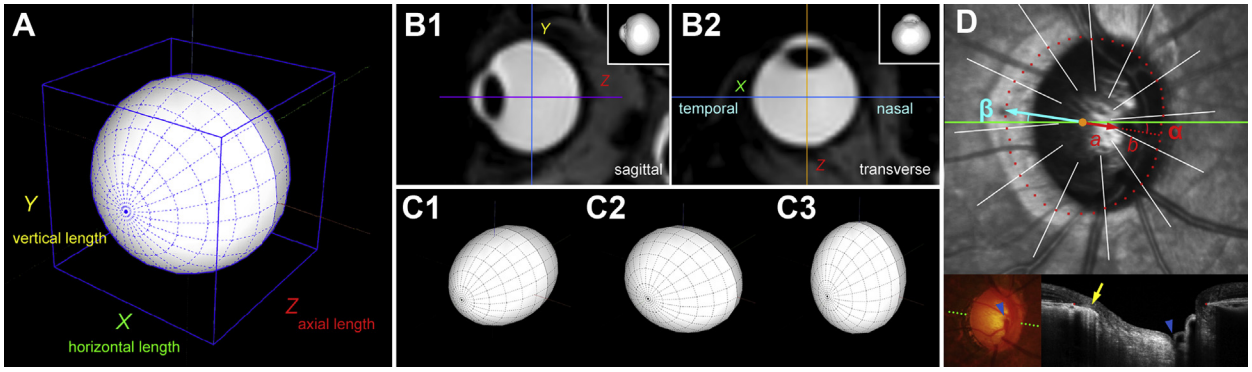

Figure 1. Grouping of 3-dimensional (3D) eyeball shape and the measurement of central retinal vascular trunk (CRVT) position. **A,** To determine the deviations from the spherical shape, the lengths were measured in the horizontal (x), vertical (y), and axial (z) directions. **B,** Three-dimensional magnetic resonance imaging (MRI) image of an eyeball. Using the 3D multiplanar reconstruction (MPR) volume-rendering tool of OsiriX, we adjusted the sectional plane across the exact center of the eyeball in the sagittal ($\mathbf{B}_1$) and coronal planes ($\mathbf{B}_2$). The lengths (x, y, z) were measured by using the built-in caliper tool and compared directly in those planes. **C,** Grouping of 3D eyeball shape: group 1 ($\mathbf{C}_1$), if longest axis was z (including x=y=z); group 2 ($\mathbf{C}_2$), if x (including x=y>z); and group 3 ($\mathbf{C}_3$), if y. **D,** Measurement of the CRVT position and angular location of the longest externally oblique border (EOB). An infrared image shows the demarcated Bruch's membrane opening (BMO; red dots) in the right eye. The orange dot indicates the BMO center, and the green line indicates the reference line. The blue arrowhead indicates the CRVT. The dotted green line indicates the location of the OCT scan. The angular deviation of the CRVT (α) was measured clockwise, with the nasal horizontal midline as 0° in the right-eye orientation (red curved line). A positive value indicated the superior location relative to the reference line, and a negative value indicated the inferior location. The angular location of the longest EOB (β, yellow arrow) was measured clockwise, with the temporal horizontal midline as 0° (blue curved line). A positive value indicated the superior location, and a negative value indicated the inferior location. From the BMO center, the distances were measured to the CRVT (a) and to the BMO margin in the same direction (b). The ratio of these distances was defined as the "shift index" (a/b), which was used to measure the extent of CRVT deviation.

determined the spherical shape group for each eyeball. In cases of disagreement, a third adjudicator (S.H.K.) was consulted to achieve consensus.

Assessment of Deep-ONH Complex

The peripapillary area was imaged by SD-OCT. The corneal curvature of each eye was entered into the SD-OCT system (Spectralis, Heidelberg Engineering) before performing SD-OCT scanning to compensate for potential magnification errors. The deep-ONH complex was imaged by using the EDI technique. The BMO was demarcated by using the Glaucoma Module Premium Edition of the Spectralis machine. With 24 high-resolution radial scan images of the ONH, 15° apart from each other, and each averaged from 24 individual B-scans, SD-OCT automatically detected the margin of the BMO. Every detected BMO margin was reviewed by one of the authors (K.M.L.), and errors were corrected manually. Based on the edited BMO margin, the Spectralis machine calculated the area and center of the BMO.

The CRVT position was measured from the BMO center as described previously.[13] First, its emergence was demarcated on the funduscopic infrared images and color-disc photography (Fig 1D); next, it was confirmed by cross-sectional SD-OCT imaging in all cases. In cases with an invisible CRVT on infrared fundus photographs and B-scan EDI SD-OCT images, either fluorescein or OCT angiography (Spectralis) was used to determine the presence of the CRVT within the BMO. The position of the CRVT was defined in 2 aspects: (1) its angular deviation (Fig 1D, α) and (2) the extent of shift (Fig 1D, a). The angle was measured based on the right-eye orientation, with the nasal horizontal midline as 0° (a positive value indicated a CRVT located superiorly, and a negative value indicated a CRVT located inferiorly). To evaluate the extent of shift, the distance of the CRVT from the center of the BMO (a) was divided by the distance of the BMO margin from the center of the BMO in that direction (b) and defined as the "shift index" (Fig 1D, a/b). In cases of invisible CRVT due to being located outside the BMO, the shift index was defined as 1.0, and the angular deviations were not determined. Those cases were excluded from the analysis of the angular location of the CRVT.

The obliquity of ONH borders was assessed as internally oblique, nonoblique, or externally oblique.[14] The presence of an EOB signifies scleral protrusion through the BMO in that meridian,[9-11] a condition also known as "γ-zone PPA."[18,19] In cases of an EOB larger than 100 μm, the angular location of the maximal width of the EOB was measured from the BMO center (Fig 1D, β), with the temporal horizontal midline as 0° (a positive value in the superior hemisphere and a negative value in the inferior hemisphere).

The Disc Ovality Index was defined as the ratio between the largest and smallest disc diameters, and the BMO Ovality Index was defined by those of the BMO diameters. The torsion degree was defined as the deviation of the long axis of the clinical disc margin from the reference line, which was set perpendicularly to the foveal-BMO axis.[5] A positive torsion value indicated inferotemporal torsion, and a negative value indicated superonasal torsion.[5] All of the measurements were performed using the Image J program (version 1.51, National Institutes of Health, Bethesda, MD) by one of the authors (K.M.L.), who was blinded to the participants' clinical information.

Data Analysis

We used Cohen's kappa to assess the inter-rater reliability of the groupings of 3D eyeball shape. The group comparisons were performed by the analysis of variance test, with post hoc Scheffe testing for the continuous variables and chi-square testing for the categoric variables. Regression analysis was used to determine the factors affecting the position of the CRVT. The generalized estimating equation regression model was applied to account for the correlation of paired eyes from the same participant. Univariable and multivariable generalized estimating equation analyses were used to determine the factors, and parameters with a P value less

Table 1. Demographic Data According to Three-Dimensional Eyeball Shape

	Group 1 (A) Prolate Sphere (N = 54)	Group 2 (B) Horizontally Oblate Sphere (N = 23)	Group 3 (C) Vertically Oblate Sphere (N = 35)	P	Post Hoc Test
Age, years	48.4 ± 14.1	67.0 ± 8.7	67.4 ± 10.9	<0.001*	A<B=C
Sex (male/female)	28/26	4/19	10/25	0.007†	
Axial length, mm	26.3 ± 1.5	23.0 ± 0.8	24.6 ± 1.2	<0.001*	A>C>B
Horizontal length on 3D MRI (*x*), mm	24.2 ± 1.3	23.2 ± 0.9	23.8 ± 1.0	0.001*	A>C=B
Vertical length on 3D MRI (*y*), mm	24.3 ± 1.2	23.0 ± 0.8	24.7 ± 1.1	<0.001*	B<A=C
Axial length on 3D MRI (*z*), mm	25.7 ± 1.5	22.4 ± 0.8	24.0 ± 1.1	<0.001*	A>C>B
IOP, mmHg	14.3 ± 2.6	14.9 ± 2.8	13.6 ± 3.2	0.255*	
BMO area, mm^2	3.32 ± 1.92	2.13 ± 0.35	2.56 ± 0.62	0.002*	A>B=C
Foveal-BMO axis, °	−6.0 ± 3.3	−7.2 ± 4.9	−7.7 ± 3.7	0.086*	
Shift index	0.72 ± 0.27	0.37 ± 0.18	0.62 ± 0.30	<0.001*	A=C>B
Angular deviation of CRVT, ° (absolute value)	32.5 ± 40.9	150.2 ± 39.6	102.7 ± 26.7	<0.001*	A<C<B
Angular location of longest EOB, ° (absolute value)	37.7 ± 28.3	130.7 ± 27.7	88.5 ± 27.8	<0.001*	A<C<B
Temporal position of CRVT	3 (6%)	21 (91%)	16 (46%)	<0.001†	
Disc Ovality Index	1.37 ± 0.24	1.16 ± 0.07	1.34 ± 0.22	0.001*	A=C>B
BMO Ovality Index	1.07 ± 0.06	1.11 ± 0.07	1.09 ± 0.06	0.033*	A<C=B
Torsional angle, ° (absolute value)	22.6 ± 24.0	19.7 ± 20.1	52.1 ± 26.3	<0.001*	A=B<C
No. of patients with glaucoma	35 (65%)	15 (65%)	20 (57%)	0.732	

BMO = Bruch's membrane opening; CRVT = central retinal vascular trunk; EOB = externally oblique border; IOP = intraocular pressure.
*Comparison performed using analysis of variance test with post hoc Scheffe test to compare differences among 3 groups.
†Comparison performed using chi-square test.

than 0.10 in the univariable analysis were included in the subsequent multivariable analysis. Statistical analyses were performed with commercially available software (Stata version 14.0; StataCorp LP, College Station, TX) and R statistical packages version 3.4.3 (available at http://www.r-project.org; assessed December 5, 2017). The data are presented as the mean ± standard deviation except where stated otherwise, and the cutoff for statistical significance was set to $P < 0.05$.

Results

This study initially involved 63 subjects who had undergone radial scans of the ONH complex and were willing to have 3D-MRI scanning. Of these, 4 subjects did not undergo the MRI scanning (3 subjects withdrew their consent, and 1 had a metallic foreign body detected during the MRI scanning). Furthermore, 2 subjects were excluded because of poor SD-OCT image quality, and 1 subject was excluded because of bifurcation of the CRVT. These exclusions resulted in a final sample of 112 eyes of 56 subjects (64 open-angle glaucoma eyes, 6 angle-closure glaucoma eyes, 42 eyes without glaucoma). The subjects were aged 58.2 ± 15.4 years and had a refractive error of −2.87 ± 3.46 diopters, and an axial length of 25.1 ± 1.8 mm; 35 of the subjects were female (63%).

The eyeballs were classified according to 3 groups based on the relative horizontal (*x*), vertical (*y*), and axial (*z*) lengths: (1) group 1, prolate sphere (54 eyes); (2) group 2, horizontally oblate sphere (23 eyes); and (3) group 3, vertically oblate sphere (35 eyes; Table 1). The grouping of the eyeballs' 3D shape showed excellent interobserver reproducibility (Kappa statistic = 0.919; 95% confidence interval, 0.856−0.982). Axial length was longer in the order of group 1, group 3, and group 2 (Table 1). Among the subjects in groups 1 to 3, the subjects in group 1 were younger and had a larger BMO area than the subjects in the other groups; the subjects in group 2 had a shorter shift index and a smaller ovality index; the subjects in group 3 had a larger torsion angle (Table 1).

The CRVT position differed among the groups (Table 1, Fig 2). Group 1 was the most frequent type of eyeball shape, representing a prolate sphere with the longest diameter in the axial direction (Fig 3C); in this group, the CRVT was located mostly on the nasal side (Figs 2A, 3A). Group 2 represented an oblate sphere with the longest diameter in the horizontal direction (Fig 4C); in this group, the CRVT was located mostly on the temporal side (Figs 2B, 4A). Group 3 represented an oblate sphere with the longest diameter in the vertical direction (Fig 5C); in this group, the CRVT positions were all close to the vertical meridian (Figs 2C, 5A, B).

The angular location of the longest EOB also differed among the groups (Table 1). The longest EOB was situated in the direction opposite to the CRVT position ($r = -0.635$, $P < 0.001$; Fig 2D): It was found mostly on the temporal side in group 1 (Fig 3B), mostly on the nasal side in group 2 (Fig 4B), and on the inferior side in group 3 (Fig 5A, B).

Some eyes showed marked asymmetry between the nasal/temporal and superior/inferior sides (Figs 6−8). In these cases, the CRVT was located on the opposite side of overgrowth: on the superotemporal side in cases of nasal and inferior overgrowth (Figs 6, 8A), on the superior side in cases of predominant inferior overgrowth (Fig 7), and on the temporal side in cases of predominant nasal overgrowth (Fig 8B).

In the generalized estimating equation analysis, the temporal location of CRVT (larger absolute value of angular deviation) was associated with older age ($P = 0.001$), nasal location of longest EOB ($P < 0.001$), and a more oblate shape of the eyeball ($P < 0.001$ for group 2, $P = 0.007$ for group 3 relative to group 1; Table 2).

Discussion

In this study, we discovered that the 3D shape of the eyeball was closely associated with the positions of the CRVT and EOB from the BMO center, which were thus associated with diverse directionalities of offset between

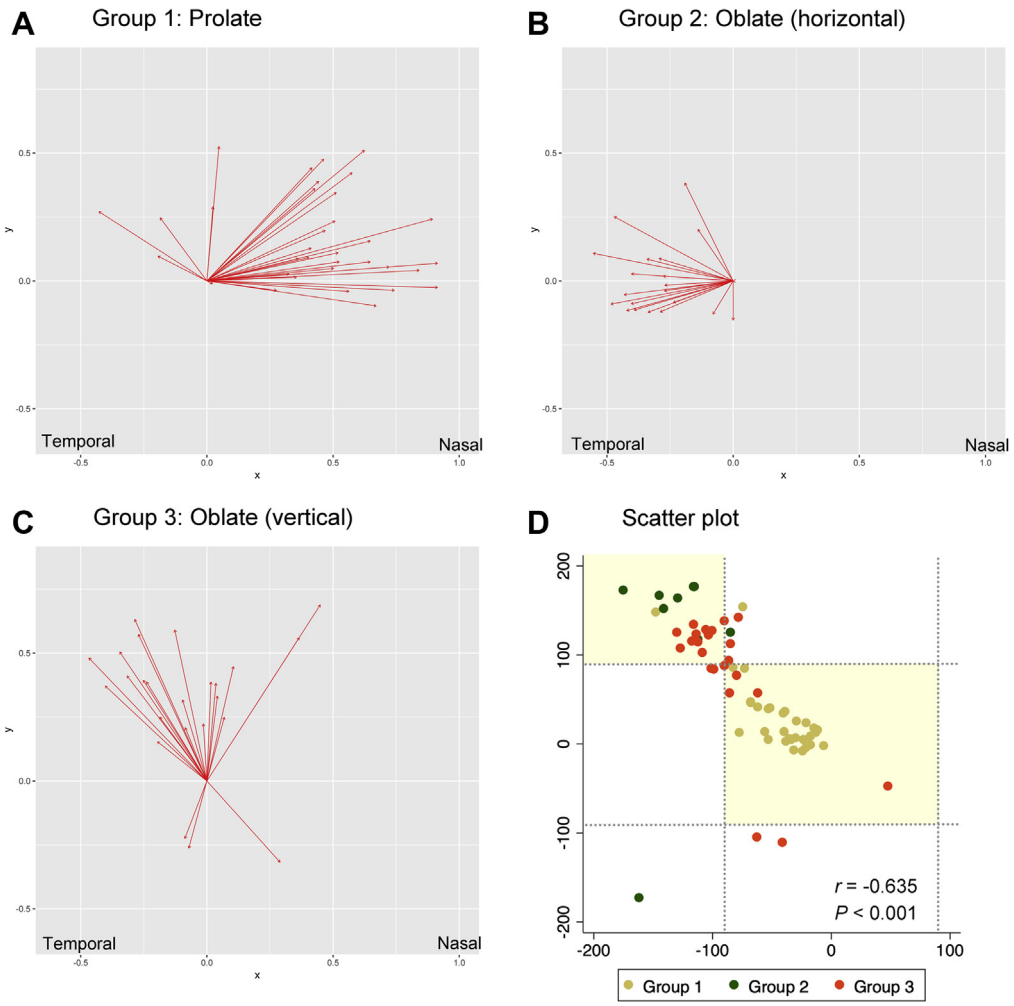

Figure 2. Locations of the central retinal vascular trunk (CRVT) and longest externally oblique border (EOB). **A–C,** Vector fields indicating the relative position of the CRVT within the Bruch's membrane opening (BMO). The length of each arrow is the shift index. The data on the left eye are flipped to the right-eye orientation. The CRVT position was predominantly on the nasal side in group 1 (**A**), on the temporal side in group 2 (**B**), and along the vertical meridian in group 3 (**C**). **D,** Scatterplot shows the relationship between the CRVT position and the angular location of the longest EOB. The longest EOB was in the direction opposite to the CRVT position ($r = -0.635$, $P < 0.001$). Reference lines are drawn at 90° and −90° to indicate the nasal and temporal sides.

the LC and BMO in adults. Half of the subjects had a prolate eyeball shape (group 1), the diameter of which is longest in the axial dimension. In these cases, the CRVTs were located mostly on the nasal side, and the longest EOB was observed on the opposite, temporal side. One-fifth of the subjects had a horizontally oblate eyeball shape (group 2), the diameter of which was longest in the horizontal dimension. These cases, in contrast to those in group 1, were associated with temporally located CRVT, and the longest EOB was on the nasal side. One-third of the subjects had a vertically oblate eyeball shape (group 3), the diameter of which is longest in the vertical dimension. The location of the CRVT was close to the vertical meridian in all cases, and the longest EOB was on the inferior side along the vertical meridian.

The ONH morphology of newborns has been reported to be highly uniform with centrally located CRVTs.[8] This finding contrasts with the diverse ONH morphology of adults. Thus, it seems reasonable to posit that this morphologic difference might be acquired during the process of eyeball growth. In the ONH, retinal and scleral layers have their own openings: the BMO and LC, respectively. If their relative position is changed, the ONH morphology can change.[9-11] In our Boramae Myopia Cohort study, we demonstrated nasal shifting of the CRVT from the BMO center and rotation of the temporal ONH border from internally to externally oblique in myopic eyes.[9-11] Because the CRVT is embedded in the dense connective tissue of the LC,[12] all of these changes suggested an LC shift nasally relative to the BMO.[9-11] Such shifting of LC from the BMO resulted in a characteristic myopic ONH appearance: oval shape, nasally located CRVT, and γ-zone PPA on the temporal side.[9-11] In this study, we found that such changes occurred predominantly in eyes with a prolate

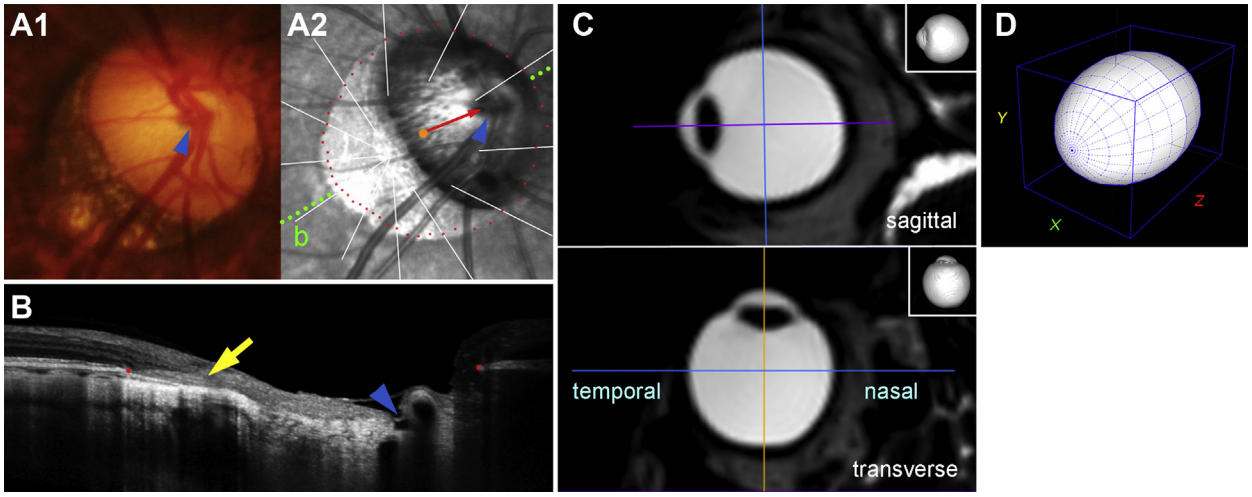

Figure 3. Sample case (right eye) for group 1. **A,** Optic nerve head (ONH) morphology. **A_1,** Disc photograph. The arrowhead indicates the location of the central retinal vascular trunk (CRVT). **A_2,** Infrared image with demarcated Bruch's membrane opening (BMO) margin (red dots). The red arrow is drawn to show the direction and the extent of CRVT (arrowhead) deviation from the BMO center (orange dot). The dotted green line indicates the location of the OCT scan. **B,** B-scan OCT image. The red dots indicate the BMO margin. Please note the externally oblique border (EOB) (yellow arrow) in the direction opposite to the CRVT deviation (arrowheads). **C,** Sagittal and transverse sectional images of 3D—magnetic resonance imaging (MRI). Because *z* was the longest, the eye was classified as group 1 (**D**, prolate sphere). Three-dimensional eyeball shapes are available in Video 1 (available at www.aaojournal.org).

sphere (group 1). During eyeball expansion, the retina and sclera face different growth scenarios: Unlike the sclera, which does not need to preserve a specific region during expansion, the retina needs to preserve the posterior polar region to retain the cellular density that is critical to BCVA.[20] Against the global expansion of the sclera, the retina, to preserve the posterior polar retinal structure, grows preferentially in the equatorial region (Fig 9, bottom left). We speculate that this discrepancy resulted in the nasal shifting of the outer wall relative to the retinal structure and BMO in the myopes (Fig 9, prolate growth).[9-11]

In this study, we also observed the mirror image of the myopic ONH in certain eyes: the CRVT position on the

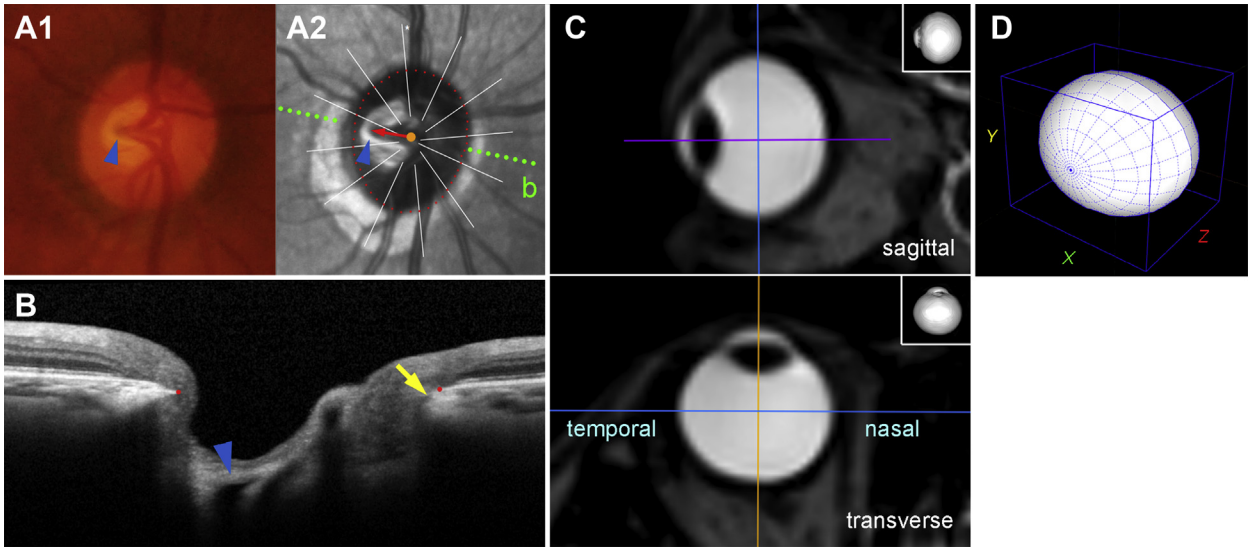

Figure 4. Sample case (right eye) for group 2. **A,** Optic nerve head morphology. **A_1,** Disc photograph. The dotted green line indicates the location of the OCT scan. **A_2,** Infrared image with demarcated Bruch's membrane opening (BMO) margin (red dots). The red arrow is drawn to show the direction and the extent of central retinal vascular trunk (CRVT) (arrowhead) deviation from the BMO center (orange dot). **B,** B-scan OCT image. The CRVT emerges on the temporal side (arrowhead) from the perspective of the BMO (red dots), and the externally oblique border (EOB) is located on the nasal side (yellow arrow). **C,** Sagittal and transverse sectional images of 3D—magnetic resonance imaging (MRI). Because *x* was the longest, the eye was classified as group 2 (**D**, horizontally oblate sphere). Oblate growth resulted in a nasal shift of the outer wall. Three-dimensional eyeball shapes are available in Video 2 (available at www.aaojournal.org).

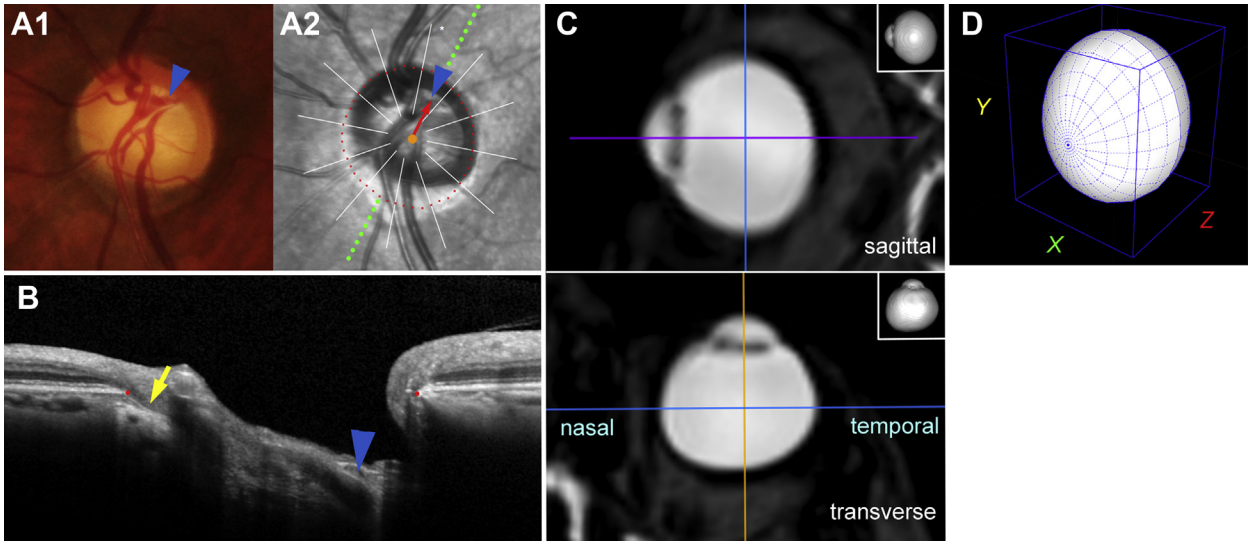

Figure 5. Sample case (left eye) for group 3. **A,** Optic nerve head morphology. **A_1,** Disc photograph. The dotted green line indicates the location of the OCT scan. **A_2,** Infrared image with demarcated Bruch's membrane opening (BMO) margin (red dots). The red arrow is drawn to show the direction and the extent of central retinal vascular trunk (CRVT) (arrowhead) deviation from the BMO center (orange dot). The dotted lines indicate the location of the OCT scans. **B,** B-scan image shows the superiorly located CRVT (arrowhead) and inferiorly located externally oblique border (EOB) (yellow arrows), both of which suggest an outer wall shift to the superior side. **C,** Sagittal and transverse sectional images of 3D—magnetic resonance imaging (MRI). In contrast to a crystalline lens, an intraocular lens appears as a thin wall. Because *y* was the longest, the eyes were classified as group 3 (**D**, vertically oblate sphere). Vertical overgrowth resulted in a superior shift of the outer wall. The superiorly located CRVT and the inferior EOB are characteristic findings of tilted disk syndrome. Three-dimensional eyeball shapes are available in Video 3 (available at www.aaojournal.org).

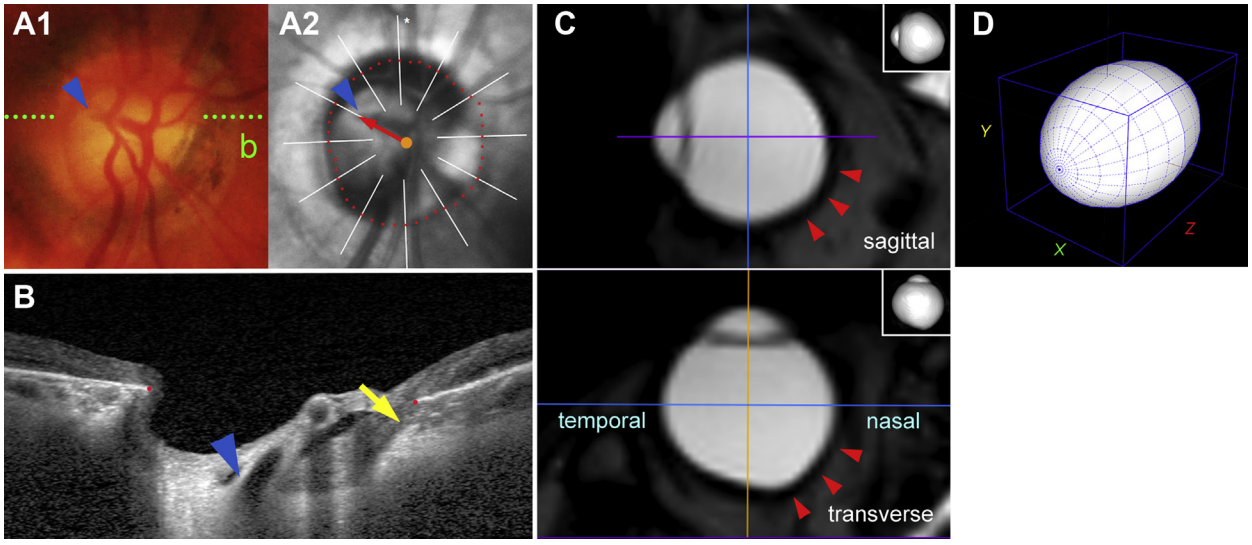

Figure 6. Sample case (right eye) of scleral asymmetry. **A_1,** Disc photograph. The arrowhead indicates the location of the central retinal vascular trunk (CRVT). The dotted green lines indicate the locations of the OCT scans. **A_2,** Infrared image with demarcated Bruch's membrane opening (BMO) margin (red dots). The red arrow is drawn to show the direction and the extent of CRVT (arrowhead) deviation from the BMO center (orange dot). **B,** B-scan image. Please note the temporally located CRVT (arrowhead) and the nasally located externally oblique border (EOB) tissue (yellow arrow). **C,** Sagittal and transverse sectional images of 3D—magnetic resonance imaging (MRI). In contrast to a crystalline lens, an intraocular lens appears as a thin wall. Because *z* was the longest, the eye was classified as group 1 (prolate sphere). Although this eyeball was classified as group 1 (**D**), there was prominent asymmetry between the nasal/temporal and the superior/inferior sides (**C**, red arrowheads). Whereas this case was counter to our initial expectation (i.e., prolate growth is related to nasal shift), it still supports our speculation that lamina cribrosa (LC) shift would be driven by outer wall shift in the direction from the overgrowth region to the undergrowth region. In this eye, the outer wall shift to the temporal side might have originated from asymmetrical growth: more growth on the nasal side may have induced the outer wall to move from the nasal to the temporal side. Three-dimensional eyeball shapes are available in Video 4 (available at www.aaojournal.org).

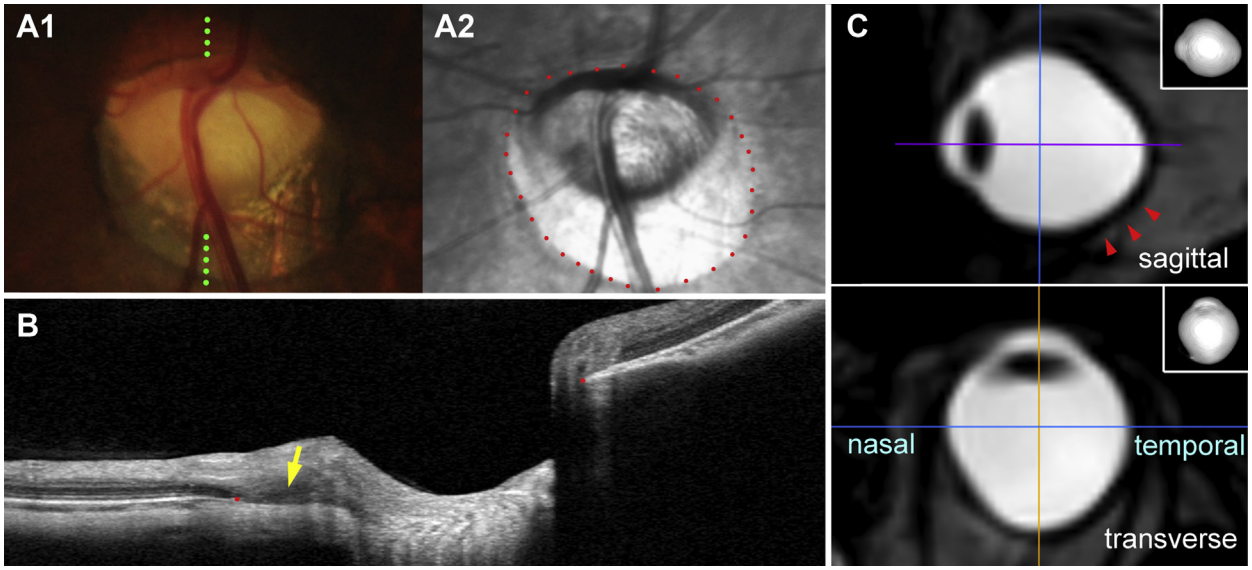

Figure 7. Sample case (left eye) of scleral asymmetry. **A_1,** Disc photographs. **A_2,** Infrared image with demarcated Bruch's membrane opening (BMO) margin (red dots). The central retinal vascular trunk (CRVT) is supposed to be along the vertical meridian but is invisible. The dotted green lines indicate the locations of the OCT scans. **B,** B-scan images. Please note the inferiorly located externally oblique border (EOB) (yellow arrow), which suggests an outer wall shift to the superior side. **C,** Three-dimensional eyeball shape. Because *z* was the longest, the eyes were classified as group 1 (prolate sphere). Although this eyeball was classified as group 1, there was prominent asymmetry between the superior/inferior sides (**C**, red arrowheads), and no such asymmetry was evident between the nasal and temporal sides. This resulted in outer wall shift in a perpendicular direction that was not deviated toward the temporal or nasal side. Three-dimensional eyeball shapes are available in Video 5 (available at www.aaojournal.org).

temporal side and the EOB on the nasal side, for which changes would be suggestive of outer wall shifting in a reverse direction, namely, temporal shift. Such changes were exclusively associated with the horizontally oblate eyeball shape (group 2). Newborns have a mean axial length of 16.8 mm.[16] This finding means that even short and hyperopic eyes in adults must have experienced eyeball expansion. Theoretically, in the case of oblate eyeball expansion, regionally disproportionate growth of the retina could lead to relative outer wall shift in a temporal direction, in contrast to a nasal direction in the case of prolate expansion (Fig 9, bottom right). Because the ONH is located slightly on the nasal side relative to the fovea, equatorial undergrowth of the inner layer is associated with a more centrifugal location of internal opening (Fig 9, oblate growth), and equatorial overgrowth of the inner layer is associated with a more centripetal location of internal opening (Fig 9, prolate growth). Therefore, prolate growth (group 1) is associated with a nasally located CRVT, and oblate growth (group 2 or 3) is associated with a temporally located CRVT (Fig 2).

In human eyes, both prolate and oblate growth have been demonstrated in MRI studies using 3D modeling.[21,22] Myopic eyes also have been reported to be associated with more hyperopic peripheral refractions[23] suggestive of the prolate eyeball shape.[24] This finding is due to the relative overgrowth in the axial dimensions in myopic eyes.[22,25,26] By contrast, emmetropic eyes and hyperopic eyes are reported to be associated with relative peripheral myopia and an oblate eyeball shape[23] due to relative overgrowth in the horizontal or vertical dimensions during eyeball expansion.[22,26] Provided that the disproportionate growth of the retina is unmatched by that of the sclera in the corresponding region, these changes would result in either a nasal or temporal shift of the outer wall of the ONH if the effect of other factors such as thinning or remodeling could be neglected.

The directionality of the CRVT position, however, was diverse in this study, as was that of the actual LC shift in the prospective study.[10] The directionality was not confined to either the nasal or the temporal direction. This finding implies that outer scleral growth might have a marked asymmetry, and that it is not a passive result of a mere expansion of the inner retinal structure (Fig 9, top). Asymmetric bulging of the vitreous chamber, rather than prolate or oblate or diffuse expansion, was reported in an animal study.[24] Likewise, highly myopic eyes occasionally have had nasally or temporally distorted shapes rather than spherical, conical, or barrel shapes.[17,27] Additionally, in this study, some eyeballs showed seemingly marked curvature differences between the nasal/temporal and superior/inferior sides (Figs 6–8). In these cases, the direction of outer wall shift was more dependent on the actual scleral shape than on the 3D eyeball shape grouping (Figs 6 and 7). The asymmetry even resulted in a difference in the CRVT positions between paired eyes of the same subject (Fig 8). To summarize, the direction of LC shift is thought to be determined by the growth patterns of both the inner retinal structure and the outer scleral structure. In symmetric expansion of the outer wall, disproportionate growth of the retina will induce a nasal shift in the case of prolate growth and a temporal shift in the case of oblate

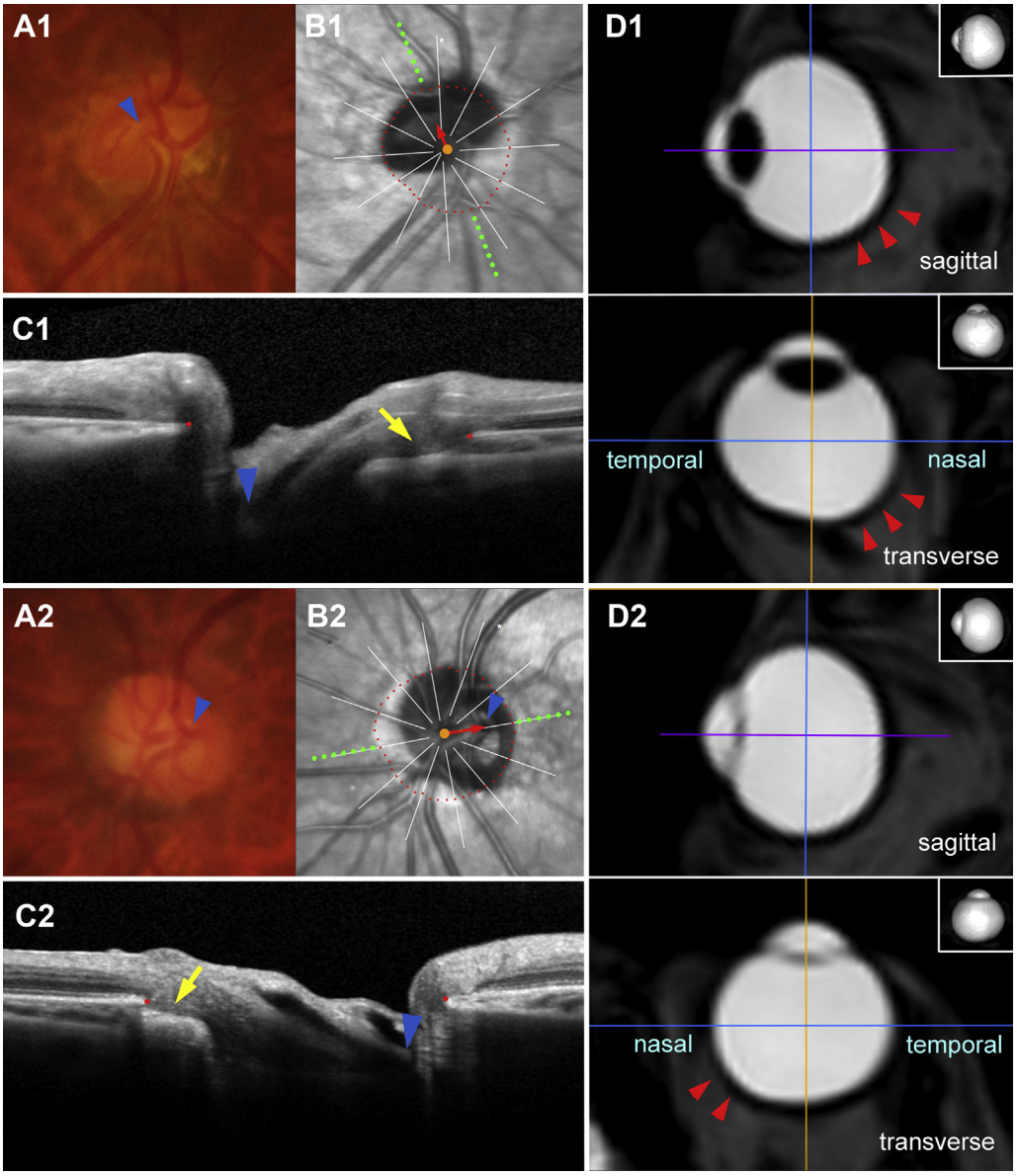

Figure 8. Sample cases of intra-individual difference. $\mathbf{A_1}$–$\mathbf{D_1}$, Right and $\mathbf{A_2}$–$\mathbf{D_2}$ left eyes of the same subject. **A,** Disc photographs. **B,** Infrared images with demarcated Bruch's membrane opening (BMO) margin (red dots). The red arrow is drawn to show the direction and the extent of central retinal vascular trunk (CRVT) (arrowhead) deviation from the BMO center (orange dot). The dotted green lines indicate the location of the OCT scans. $\mathbf{C_1}$, For the right eye, the B-scan image shows a superiorly located CRVT (arrowhead) and an inferiorly located externally oblique border (EOB) (yellow arrow), both of which suggest an outer wall shift to the superior side. $\mathbf{C_2}$, For the left eye, the B-scan image shows temporally located CRVT (arrowhead) and nasally located EOB (yellow arrow), both of which are suggestive of outer wall shift to the temporal side. **D,** Three-dimensional eyeball shapes. The right eye is phakic, and the left eye is pseudophakic. The right eye was classified as group 3 with prominent nasal/temporal and superior/inferior asymmetry ($\mathbf{D_1}$, red arrowheads); the left eye was classified as group 2 with a lesser degree of nasal/temporal asymmetry ($\mathbf{D_2}$, red arrowheads). This classification indicates that the direction of shift could differ between paired eyes of the same individual, and that it is more dependent on the 3D shape of the eyeball. Three-dimensional eyeball shapes are available in Video 6 (available at www.aaojournal.org).

growth. In asymmetric expansion of the outer wall, however, the direction of LC shift is more directly dependent on the scleral growth direction: from the overgrowth region to the undergrowth region (Fig 9).

Although asymmetric growth occurred in all directions of LC shift, it was observed more frequently in cases of superior directionality (Figs 6–8). We speculate that this was due to the inferior location of the embryonic fissure. Tilted disk syndrome, which is the inferonasal rotation of the optic disk with a contiguous inferonasal crescent; thinning or atrophy of the retinal pigment epithelium and choroid; posterior staphyloma of the affected area; and situs inversus of the retinal vessels[28] have been thought to be within the spectrum of ocular coloboma.[28,29] Likewise, in the case of the gross defective closure of the coloboma, some eyes may have a microscopically defective structure inferiorly.

Table 2. Factors Associated with Angular Location of Central Retinal Vascular Trunk in Single Hemisphere*

	Univariable Analysis			Multivariable Analysis†		
	Coefficient	*95% CI*	*P*	*Coefficient*	*95% CI*	*P*
Age, years	**2.675**	**(1.799–3.551)**	**<0.001**	**0.903**	**(0.349–1.456)**	**0.001**
Female (vs. male sex)	32.999	(−1.881 to 67.878)	0.064	9.764	(−4.326 to 23.854)	0.174
Axial length, mm	−21.610	(−28.616 to −14.604)	<0.001	−0.195	(−5.100 to 4.710)	0.938
IOP, mmHg	−1.137	(−6.268 to 3.994)	0.664			
BMO area, mm^2	−5.843	(-14.508, 2.822)	0.186			
BMO Ovality Index	−1.530	(−126.749 to 123.689)	0.981			
Foveal-BMO axis, °	−1.678	(−3.521 to 0.165)	0.074	−0.163	(−1.255 to 0.929)	0.770
Shift Index	−35.678	(−90.892, 19.536)	0.205			
Angular location of longest EOB, ° (absolute value)	**1.122**	**(0.948–1.297)**	**<0.001**	**0.521**	**(0.285–0.757)**	**<0.001**
Eyeball shape (vs. prolate sphere)						
Horizontally oblate sphere	**114.197**	**(93.112–135.283)**	**<0.001**	**65.429**	**(39.557–91.300)**	**<0.001**
Vertically oblate sphere	**62.922**	**(42.936–82.907)**	**<0.001**	**23.884**	**(6.429–41.339)**	**0.007**

BMO = Bruch's membrane opening; CI = confidence interval; CRVT = central retinal vascular trunk; EOB = externally oblique border; IOP = intraocular pressure; OR = odds ratio.
Statistically significant values ($P < 0.05$) are shown in bold.
*Angular location of CRVT was measured in absolute value to represent the location within a single hemisphere.
†Variables with $P < 0.10$ in the univariable analysis were included in the subsequent multivariable analysis.

Those structures would be stretched differently during eyeball expansion and result in scleral bulging along the vertical midline with a marked regional asymmetry of the sclera. In those eyes, overgrowth of the inferior sclera and subsequent superior LC shift could occur. Repetitive mechanical loading on the ocular globe via the optic nerve sheath might be another cause of acquired scleral deformation.[30] Further longitudinal study is required to elucidate whether scleral growth shows marked asymmetry in such eyes, as we have speculated in this study.

We measured the entire eyeball shape, not a curvature of limited range; the former could be imaged only by MRI, and the latter could also be imaged by OCT. Because not only a regional protrusion but also an entire eyeball shape (prolate or oblate sphere) is important in determining relative shifting between layers, we had to use a 3D-MRI in this study. In addition, care should be taken when interpreting posterior polar shape as measured by OCT. During OCT imaging, the length of light differs according to whether it is directed to the fovea or the peripheral retina, because it is swept across the curved plane from a common pivot point. Therefore, the contour obtained by OCT is, without adequate optical correction, affected by marked distortion in the peripheral retina.[31,32] We could have avoided those problems by using 3D-MRI.

Notably, what we measured by T2-weighted 3D-MRI was a fluid-filled space within the eye rather than the eyeball, as indicated by the axial length difference measured by IOL-Master and 3D-MRI (Table 1); the mean difference of 0.6 mm represented the central corneal thickness, which was included during measurement by the former but not by the latter. Therefore, its shape, as determined, was related to the vitreous/retinal—not the sclera/orbital fat—interface. However, the mean difference was consistently 0.6 mm among the groups, which reflected that although we measured the fluid-filled cavity, not the eyeball, the measurement was reliable. T2-weighted 3D-MRI scanning has been used in many studies to measure 3D eyeball shape.[17,21,26,27] We speculated that the preference for T2-weighted images is due to the excellent contrast of the vitreous/retinal interface as imaged by the T2-weighted MRI. For further evaluation, however, additional information regarding scleral shape might enhance the understanding of the shape of the multilayer 3D eyeball.

Our study has 2 clinical implications. First, it provides one possible explanation of the various positions of the CRVT and of the EOB in the aspect of deviation from the eyeball's spherical shape. The 3D shape of the eyeball is associated with the modes of eyeball expansion (prolate, oblate, asymmetric growth) and subsequent LC shift in various directions (Fig 9). Second, and more importantly, this study's results provide new insights into funduscopic disc examination: The more dysplastic the disc, the greater the eyeball deformation. Therefore, when we performed funduscopic examinations, we could image the entire hidden eyeball shape, which is associated with ONH morphology and possibly related to a more stressful environment for the RGC axons.

Study Limitations

First, both glaucoma patients and healthy subjects were included, implying a possible confounding effect of LC remodeling on the CRVT position in glaucomatous eyes. However, glaucomatous ONH change has been reported not to affect the position of the CRVT in the LC portion.[33,34] Moreover, our subgroup analysis after excluding glaucomatous eyes also showed very similar results (Tables S1 and S2, available at www.aaojournal.org). The LC change to glaucoma might be greater in the peripheral area than in the central area because the former has a larger pore size and less densely packed connective tissue than the latter.[12] Accordingly, subsequent remodeling would also be greater in the peripheral area than in the central

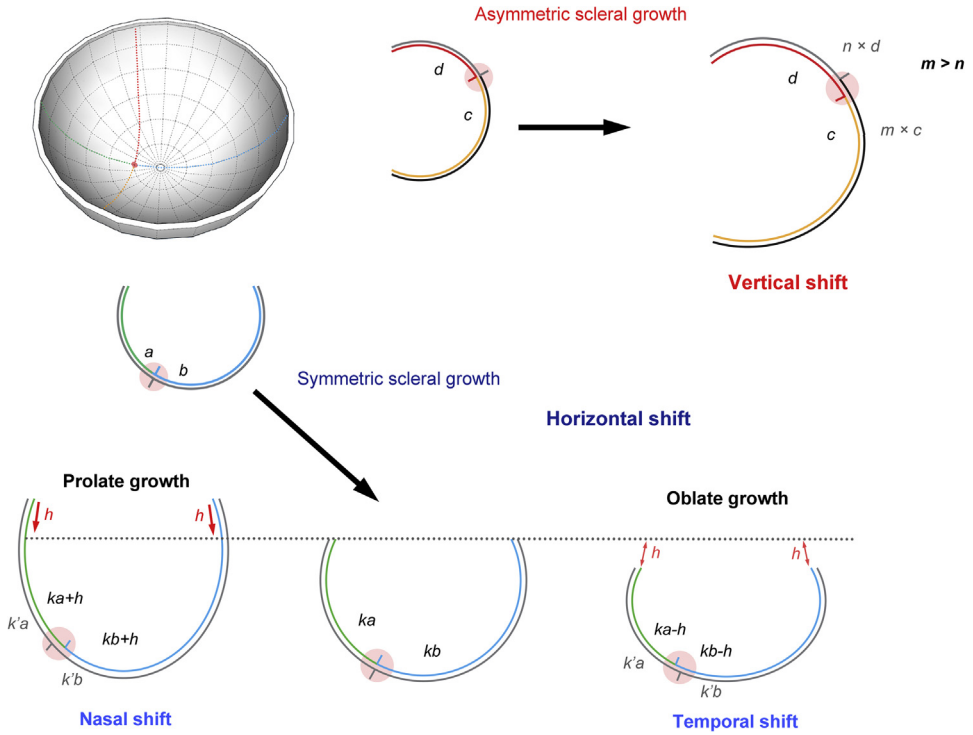

Figure 9. Presumptive mechanism of outer wall shift. Two sectional planes were drawn on a sphere: a green-blue dotted line along the horizontal line connecting the fovea and the Bruch's membrane opening (BMO), and a red-orange dotted line perpendicularly to the previous line (**top left**). If the retina grows disproportionately and the sclera grows symmetrically (**bottom**), prolate growth will move the neural canal opening (NCO) to the more centrifugal direction, and oblate growth will move the NCO to the more centripetal direction. The retina and sclera are demarcated by the green-blue and gray lines, respectively. The posterior curve of the eyeball was divided into the nasal part (green line, curved length = *a*) and the temporal part (blue line, curved length = *b*) by the optic nerve head (ONH) (red circle). The alignment of the BMO (inward bar) and the NCO (outward bar) would not be changed if the retina and sclera expanded to the same extent (*k* times, **bottom middle**). Outer wall shift, however, occurs because the retina grows with a marked regional difference to preserve the cellular density at the posterior pole, which is critical to the maintenance of best-corrected visual acuity (BCVA). For this purpose, the growth prevails in the pre- and equatorial regions of the retina and it does not in those of the sclera. If the eyeball expands symmetrically along the axial axis, a prolate sphere could be modeled by the relative retinal overgrowth in the equatorial region (*h*), which is unmatched by the scleral growth (**bottom left**). In this case, the NCO center would be located at a more centrifugal site relative to the BMO center during prolate growth (Appendix A, available at www.aaojournal.org). By contrast, an oblate sphere could be understood as the shortage of equatorial lengthening (*h*) relative to scleral expansion (**bottom right**). In this case, the NCO center would be located at a more centripetal site relative to the BMO center during oblate growth (Appendix B, available at www.aaojournal.org). If the sclera grows asymmetrically, the direction of outer wall shift is more direct: from the overgrowth region to the undergrowth region (**top right**). The markedly asymmetric scleral growth between the superior and inferior hemispheres is associated with the outer wall shift in the vertical direction (group 3).

area, and remodeling in the periphery occurs in the perpendicular direction when observed from the funduscopic view: the insertion sites move posteriorly along the neural canal.[35,36] Therefore, the CRVT position in the enface view, which is not affected by posterior migration of the LC insertion sites, would be affected only minimally by LC remodeling; thus, any confounding effect of glaucoma would be negligible. Second, we used both eyes from the same subject despite the possibility of intra-individual correlation. Being a prospective study, it was somewhat difficult to enroll a large number of participants. Statistical analysis, however, was performed while considering the paired-eye correlations. Further, the CRVT positions were markedly different, even between paired eyes of the same subject, according to the eyeball shape (Fig 8). Therefore, possible intra-individual correlations would not affect our conclusions. Third, the study design was cross-sectional; thus, we could not demonstrate serial ONH change during actual eyeball expansion. Further longitudinal study would be required to confirm our hypothesis. Fourth, all of the participants were South Korean, and there may be ethnic differences in ONH or eyeball shape.[22] Further research should investigate whether this relationship between eyeball shape and ONH morphology is replicated for different populations. Finally, our methodology for the grouping of the 3D shape of the eyeball has a limitation: it is valid for conjecturing on the general spherical shape of an eyeball but is less than ideal in its representation of regional asymmetric growth. Further research is required for a more thorough evaluation of the regional asymmetry of the outer wall growth and its implications.

In conclusion, the 3D shape of the eyeball was associated with diverse directionalities of the positions of the CRVT and EOB. Various modes of eyeball expansion during

growth may result in diverse directions of offset between the LC and the BMO in adults, which is associated with a higher susceptibility to glaucoma in certain subsets of patients.

Footnotes and Disclosures

Originally received: March 23, 2020.
Final revision: August 12, 2020.
Accepted: August 31, 2020.
Available online: September 8, 2020. Manuscript no. D-20-00634.

[1] Department of Ophthalmology, Seoul National University College of Medicine, Seoul, Korea.

[2] Department of Ophthalmology, Seoul National University Boramae Medical Center, Seoul, Korea.

[3] Department of Radiology, Seoul National University College of Medicine, Seoul, Korea.

[4] Department of Radiology, Seoul National University Boramae Medical Center, Seoul, Korea.

[5] Department of Ophthalmology, Dongguk University Ilsan Hospital, Goyang, Korea.

[6] Department of Biostatistics, Seoul National University Boramae Medical Center, Seoul, Korea.

*K.M.L. and S.-W.P. equally contributed to the work and should be considered as equivalent authors.

Disclosure(s):
All authors have completed and submitted the ICMJE disclosures form.
The author(s) have no proprietary or commercial interest in any materials discussed in this article.

Supported by a clinical research grant-in-aid from the Seoul National University Boramae Medical Center (grant no. 03-2019-23). The funders had no role in the study design, data collection and analysis, decision to publish, or preparation of the manuscript.

HUMAN SUBJECTS: Human subjects were included in this study. The human ethics committees at the Seoul National University Boramae Medical Center approved the study. All research adhered to the tenets of the Declaration of Helsinki. All participants provided informed consent.
No animal subjects were used in this study.

Author Contributions:

Conception and design: K.M. Lee, S-W. Park, S.H. Kim

Data collection: K.M. Lee, S-W. Park, S.H. Kim

Analysis and interpretation: K.M. Lee, M. Kim, S. Oh, S.H. Kim

Obtained funding: K.M. Lee, S.H. Kim

Overall responsibility: K.M. Lee, S.H. Kim

Abbreviations and Acronyms:
BCVA = best-corrected visual acuity; **BMO** = Bruch's membrane opening; **CRVT** = central retinal vascular trunk; **EDI** = enhanced depth imaging; **EOB** = externally oblique border; **LC** = lamina cribrosa; **MPR** = multiplanar reconstruction; **MRI** = magnetic resonance imaging; **NCO** = neural canal opening; **ONH** = optic nerve head; **PPA** = parapapillary atrophy; **RGC** = retinal ganglion cell; **SD** = spectral-domain; **3D** = 3-dimensional.

Keywords:
Optic nerve head morphology, Eyeball shape, 3D-MRI, Lamina cribrosa shift, Central retinal vascular trunk, Externally oblique border, Bruch's membrane opening, Boramae Myopia Cohort Study.

Correspondence:
Seok Hwan Kim, MD, Department of Ophthalmology, Seoul National University Boramae Medical Center, 39 Boramae Road, Dongjak-gu, 07061, Seoul, Korea. E-mail: xcski@hanmail.net.

References

1. Ramrattan RS, Wolfs RC, Jonas JB, et al. Determinants of optic disc characteristics in a general population: The Rotterdam Study. *Ophthalmology*. 1999;106:1588−1596.
2. Jonas JB, Budde WM. Diagnosis and pathogenesis of glaucomatous optic neuropathy: morphological aspects. *Prog Retin Eye Res*. 2000;19:1−40.
3. Jonas JB, Budde WM, Nemeth J, et al. Central retinal vessel trunk exit and location of glaucomatous parapapillary atrophy in glaucoma. *Ophthalmology*. 2001;108:1059−1064.
4. Jonas JB, Martus P, Budde WM, et al. Small neuroretinal rim and large parapapillary atrophy as predictive factors for progression of glaucomatous optic neuropathy. *Ophthalmology*. 2002;109:1561−1567.
5. Park HY, Lee K, Park CK. Optic disc torsion direction predicts the location of glaucomatous damage in normal-tension glaucoma patients with myopia. *Ophthalmology*. 2012;119:1844−1851.
6. Choi JA, Park HY, Shin HY, Park CK. Optic disc tilt direction determines the location of initial glaucomatous damage. *Invest Ophthalmol Vis Sci*. 2014;55:4991−4998.
7. Lee KS, Lee JR, Kook MS. Optic disc torsion presenting as unilateral glaucomatous-appearing visual field defect in young myopic Korean eyes. *Ophthalmology*. 2014;121:1013−1019.
8. Kim M, Kim SY, Lee KM, et al. Position of central vascular trunk and shape of optic nerve head in newborns. *Invest Ophthalmol Vis Sci*. 2019;60:3381−3387.
9. Kim M, Choung HK, Lee KM, et al. Longitudinal changes of optic nerve head and peripapillary structure during childhood myopia progression on OCT: Boramae Myopia Cohort Study Report 1. *Ophthalmology*. 2018;125:1215−1223.
10. Lee KM, Choung HK, Kim M, et al. Positional change of optic nerve head vasculature during axial elongation as evidence of lamina cribrosa shifting: Boramae Myopia Cohort Study Report 2. *Ophthalmology*. 2018;125:1224−1233.
11. Lee KM, Choung HK, Kim M, et al. Change of beta-zone parapapillary atrophy during axial elongation: Boramae Myopia Cohort Study Report 3. *Invest Ophthalmol Vis Sci*. 2018;59:4020−4030.
12. Quigley HA, Addicks EM. Regional differences in the structure of the lamina cribrosa and their relation to glaucomatous optic nerve damage. *Arch Ophthalmol*. 1981;99:137−143.
13. Lee KM, Kim M, Oh S, Kim SH. Position of central retinal vascular trunk and preferential location of glaucomatous damage in myopic normal-tension glaucoma. *Ophthalmol Glaucoma*. 2018;1:32−43.
14. Reis AS, Sharpe GP, Yang H, et al. Optic disc margin anatomy in patients with glaucoma and normal controls with spectral domain optical coherence tomography. *Ophthalmology*. 2012;119:738−747.

15. Shang K, Hu X, Dai Y. Morphological features of parapapillary beta zone and gamma zone in chronic primary angle-closure glaucoma. *Eye (Lond)*. 2019;33:1378–1386.
16. Gordon RA, Donzis PB. Refractive development of the human eye. *Arch Ophthalmol*. 1985;103:785–789.
17. Guo X, Xiao O, Chen Y, et al. Three-dimensional eye shape, myopic maculopathy, and visual acuity: the Zhongshan Ophthalmic Center-Brien Holden Vision Institute High Myopia Cohort Study. *Ophthalmology*. 2017;124:679–687.
18. Dai Y, Jonas JB, Huang H, et al. Microstructure of parapapillary atrophy: beta zone and gamma zone. *Invest Ophthalmol Vis Sci*. 2013;54:2013–2018.
19. Kim M, Kim TW, Weinreb RN, Lee EJ. Differentiation of parapapillary atrophy using spectral-domain optical coherence tomography. *Ophthalmology*. 2013;120:1790–1797.
20. Jonas JB, Ohno-Matsui K, Holbach L, Panda-Jonas S. Retinal pigment epithelium cell density in relationship to axial length in human eyes. *Acta Ophthalmol*. 2017;95:e22–e28.
21. Singh KD, Logan NS, Gilmartin B. Three-dimensional modeling of the human eye based on magnetic resonance imaging. *Invest Ophthalmol Vis Sci*. 2006;47:2272–2279.
22. Lim LS, Matsumura S, Htoon HM, et al. MRI of posterior eye shape and its associations with myopia and ethnicity. *Br J Ophthalmol*. 2020;104:1239–1245.
23. Mutti DO, Sholtz RI, Friedman NE, Zadnik K. Peripheral refraction and ocular shape in children. *Invest Ophthalmol Vis Sci*. 2000;41:1022–1030.
24. Stone RA, Flitcroft DI. Ocular shape and myopia. *Ann Acad Med Singapore*. 2004;33:7–15.
25. Atchison DA, Jones CE, Schmid KL, et al. Eye shape in emmetropia and myopia. *Invest Ophthalmol Vis Sci*. 2004;45:3380–3386.
26. Lim LS, Yang X, Gazzard G, et al. Variations in eye volume, surface area, and shape with refractive error in young children by magnetic resonance imaging analysis. *Invest Ophthalmol Vis Sci*. 2011;52:8878–8883.
27. Moriyama M, Ohno-Matsui K, Hayashi K, et al. Topographic analyses of shape of eyes with pathologic myopia by high-resolution three-dimensional magnetic resonance imaging. *Ophthalmology*. 2011;118:1626–1637.
28. Apple DJ, Rabb MF, Walsh PM. Congenital anomalies of the optic disc. *Surv Ophthalmol*. 1982;27:3–41.
29. Witmer MT, Margo CE, Drucker M. Tilted optic disks. *Surv Ophthalmol*. 2010;55:403–428.
30. Demer JL. Optic nerve sheath as a novel mechanical load on the globe in ocular duction. *Invest Ophthalmol Vis Sci*. 2016;57:1826–1838.
31. Kuo AN, McNabb RP, Chiu SJ, et al. Correction of ocular shape in retinal optical coherence tomography and effect on current clinical measures. *Am J Ophthalmol*. 2013;156:304–311.
32. Kuo AN, Verkicharla PK, McNabb RP, et al. Posterior eye shape measurement with retinal OCT compared to MRI. *Invest Ophthalmol Vis Sci*. 2016;57:196–203.
33. Wang B, Lucy KA, Schuman JS, et al. Location of the central retinal vessel trunk in the laminar and prelaminar tissue of healthy and glaucomatous eyes. *Sci Rep*. 2017;7:9930.
34. Lee KM, Kim M, Oh S, Kim SH. Hemisphere opposite to vascular trunk deviation is earlier affected by glaucomatous damage in myopic high-tension glaucoma. *PLoS One*. 2020;15:e0233270.
35. Crawford Downs J, Roberts MD, Sigal IA. Glaucomatous cupping of the lamina cribrosa: a review of the evidence for active progressive remodeling as a mechanism. *Exp Eye Res*. 2011;93:133–140.
36. Yang H, Reynaud J, Lockwood H, et al. The connective tissue phenotype of glaucomatous cupping in the monkey eye: Clinical and research implications. *Prog Retin Eye Res*. 2017;59:1–52.